




## The effect of two different substituted atoms in lithium positions on the structure of garnet-type solid electrolytes

Sevda SARAN<sup>1,\*</sup>, Osman Murat ÖZKENDİR<sup>2</sup>, Ülfet ATAV<sup>1</sup>

<sup>1</sup>Department of Physics, Faculty of Science, Selçuk University, Konya, Turkey

<sup>2</sup>Department of Natural and Mathematical Sciences, Faculty of Engineering, Tarsus University, Mersin, Turkey

Received: 10.12.2020

Accepted/Published Online: 08.06.2021

Final Version: 28.06.2021

**Abstract:**  $\text{Li}_7\text{La}_3\text{Zr}_2\text{O}_{12}$  (LLZO), lithium lanthanum zirconate is a promising garnet-type solid electrolyte that is being intensively studied for solid-state lithium batteries. The properties of LLZO such as compatibility with the lithium electrode, stability, and ionic conductivity make them to be used in all solid-state batteries. Moreover, lithium ion concentration and distribution, doping different cations, chemical composition, and interaction between different dopants have remarkable effects on the ionic conduction of LLZO material. Herein, we investigate the solid electrolyte,  $\text{Li}_{6.4}(\text{Ga}_{(1-y)}\text{In}_{(y)})_{0.2}\text{La}_3\text{Zr}_2\text{O}_{12}$  ( $y = 0.05, 0.10, 0.15, 0.20$ ), by probing the influence of indium substitution to gallium sites at the same lithium concentration on the structure and the lithium ion conduction. A conventional solid state route, ball milling was used to synthesize the materials. Crystal structure, morphology, ionic conduction, and local electronic structure were analysed by X-ray diffraction (XRD), scanning electron microscopy (SEM), electrochemical impedance spectroscopy (EIS) and X-ray absorption fine structure (XAFS) techniques, respectively. The results revealed that the existence of indium effected the conduction adversely, although made no significant changes on the local structure.

**Key words:** Garnet-type solid electrolytes, solid electrolytes, all solid-state batteries

### 1. Introduction

The distribution of lithium ions in the  $\text{Li}_7\text{La}_3\text{Zr}_2\text{O}_{12}$  (LLZO) structure is the key factor affecting the crystal structure and thus conductivity. The first phase of LLZO is tetragonal, and it crystallizes in the I41/acd space group displays an ordered distribution of lithium (Li) ions [1]. Cubic LLZO which is the second phase, on the other hand, has an irregular Li ion distribution due to the lack of lithium in the structure and can crystallize in two different space groups (Ia-3d and I-43d) according to the effect of the substituted element [2]. In the tetragonal LLZO skeleton, Li ions occupy 3 different positions: tetrahedral 8a and octahedral 16f and 32g [3,4]. On the other hand, the cubic LLZO structure consists of dodecahedron  $\text{LaO}_8$  (24c) and octahedron  $\text{ZrO}_6$  (16a) scaffold. In the Ia-3d space group Li ions occupy the tetrahedral (24d) and octahedral (48g and 96h) sites [4]. While in the I-43d space group Li ions occupy the tetrahedral (12a,12b) and octahedral (48e) sites [5,6].

Many studies have shown that different cations substituted to  $\text{Li}^+$  positions prefer to take place at different  $\text{Li}^+$  sites. A previous study has shown that  $\text{Al}^{3+}$  ions substituted to the  $\text{Li}^+$  positions occupy the tetrahedral 24d and octahedral 96h sites [7]. On the other hand,  $\text{Ga}^{3+}$  ions prefer to sit only at 96 h sites [8]. Figure 1 shows the cubic LLZO crystal structure (a), the local structure of  $\text{Li}^+$  vacancy distribution in

\*Correspondence: sevdaaktas@selcuk.edu.tr

the un-doped (b), and Ga-doped LLZO crystal (c). In this structure,  $\text{Li}^+$  ions are randomly distributed in tetrahedral  $\text{LiO}_4$  and octahedral  $\text{Li}_2\text{O}_6$  positions. When Ga is added to the structure, Ga prefers to be in tetrahedral  $\text{LiO}_4$  positions, creating two more  $\text{Li}^+$  ion vacancies around it [9].

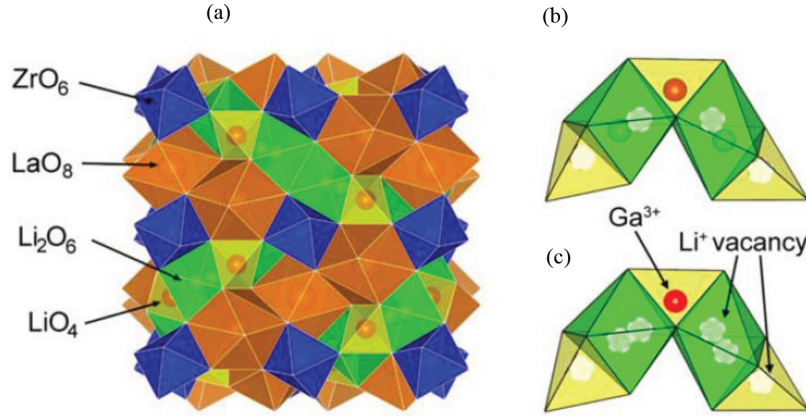


**Figure 1.** (a) The crystal structure of cubic LLZO (b) the local structure of  $\text{Li}^+$  vacancy distribution in the un-doped LLZO crystal (c) the local structure of  $\text{Li}^+$  vacancy distribution in the Ga-doped LLZO crystal.

It is stated in the literature that Ga-doped LLZO has a higher ionic mobility and conductivity than Al-doped LLZO due to the site preference and the bigger ionic radius size of  $\text{Ga}^{3+}$  [10]. Moreover, the amount of substituted atoms and the synthesis methods also have an effect on which sites the atoms occupy. To explain this situation, the study in which Al and Ta atoms are doped together can be given as an example. The co-doping of Ta atoms shifted the  $\text{Al}^{3+}$  ions to 96h positions and consequently, the  $\text{Li}^+$  ion dynamics were increased by reducing the  $\text{Li}^+$  ion diffusion paths blocked by immobilized  $\text{Al}^{3+}$  ions [11]. How the substituted elements on Li sites have an effect on the density of the structure is also as a great parameter as site preferences of the substituted elements for the  $\text{Li}^+$  ion conductivity. It is reported in the literature that the existence of  $\text{Al}^{3+}$  on the  $\text{Li}^+$  sites helps to get a dense LLZO structure [10]. Furthermore, with different co-doped elements such as Ba-Ta [12], Y-Sb [13], Al-Mn [14], Ga-Nb [15], Al-Ga [16], it has been approved that although doping has a very important contribution to  $\text{Li}^+$  ion dynamics, the interaction of different substituted atoms with each other have a great effect on the properties of the final product. Since the Ga doping provides a high conductivity, Ga was preferred in this study. Ga and In are in the same column and their ionization states are similar. Having the same number of valence electrons (Ga ( $[\text{Ar}] 3d^{10} 4s^2 4p^1$ ) and In ( $[\text{Kr}] 4d^{10} 5s^2 5p^1$ )) will enable them to replace with each other electronically. However, different quantum symmetry of In will affect the interaction of Li ions with their environment, consequently while preserving crystal structure, In may be an influence on the  $\text{Li}^+$  conductivity. That's why In and Ga atoms were doped simultaneously to the  $\text{Li}^+$  sites. Here, the concentration of  $\text{Li}^+$  ion vacancies in the structure were kept constant by keeping the total amount of doped atoms constant and what kind of changes will occur in the structure in partial replacement of Ga atoms with In atoms was investigated.

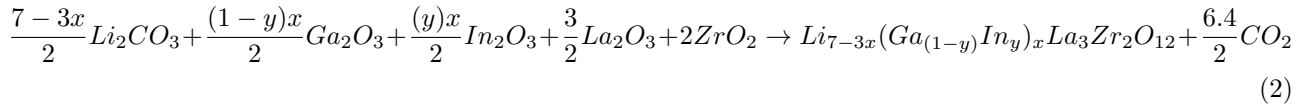
The Li ion conductivity ( $\sigma$ ) of the LLZO crystal can be expressed by the following equation.

$$\sigma = en_c\mu \quad (1)$$

Here,  $e$  is the fundamental charge,  $n_c$  is the concentration of mobile  $\text{Li}^+$  ions, and  $\mu$  is the  $\text{Li}^+$  ion mobility [17]. Consequently, since the fundamental charge is constant, the conductivity depends on the concentration and mobility of  $\text{Li}^+$  ions. In this study, since the  $\text{Li}^+$  ion concentration was also kept constant, how the partially added In atoms in place of Ga atoms affect the  $\text{Li}^+$  mobility was examined.

## 2. Experimental work

$\text{Li}_{7-3x}(\text{Ga}_{(1-y)}\text{In}_{(y)})_x\text{La}_3\text{Zr}_2\text{O}_{12}$  ( $x=0.20$ ;  $y=0.05, 0.10, 0.15, 0.20$ ) samples were synthesized by ball milling method. For the synthesis  $\text{Li}_2\text{CO}_3$  (purity: 99.9%) (10% of excess of  $\text{Li}_2\text{CO}_3$  was added to compensate Li loss during sintering time),  $\text{La}_2\text{O}_3$  (purity: 99.9%),  $\text{Ga}_2\text{O}_3$  (purity: 99.9%),  $\text{In}_2\text{O}_3$  (purity: 99.9%) and  $\text{ZrO}_2$  (purity: 99.9%) were weighted in the desired stoichiometric ratio according to the following chemical equation,



Since the oxidation state of Ga and In is +3, when  $x$  amount of in total Ga and In is substituted to the  $\text{Li}^+$  sites,  $3x$  amount of Li must be removed from the structure to balance the excess cation charge. For example, when  $x = 0.20$ , we get the  $\text{Li}_{6.4}(\text{Ga}_{(1-y)}\text{In}_{(y)})_{0.20}\text{La}_3\text{Zr}_2\text{O}_{12}$  chemical formula. Furthermore, when the  $y = 0.05, 0.10, 0.15, 0.20$  values are considered, stoichiometric ratios of the structure take the forms  $\text{Li}_{6.64}\text{Ga}_{0.19}\text{In}_{0.01}\text{La}_3\text{Zr}_2\text{O}_{12}$ ,  $\text{Li}_{6.64}\text{Ga}_{0.18}\text{In}_{0.02}\text{La}_3\text{Zr}_2\text{O}_{12}$ ,  $\text{Li}_{6.64}\text{Ga}_{0.17}\text{In}_{0.03}\text{La}_3\text{Zr}_2\text{O}_{12}$ ,  $\text{Li}_{6.64}\text{Ga}_{0.16}\text{In}_{0.04}\text{La}_3\text{Zr}_2\text{O}_{12}$ , respectively. Here, In is added to the structure by decreasing the Ga amount, but total amount of Ga and In is kept constant (equal to 0.20).

Powders were mixed, ball milled for 12 h, and heated at 500 °C in air for 6 h. At the second and third steps the same processes were applied to the samples with different temperature degrees and milling and heating times as the follow; at second step powders were ball milled for 6 h then heated at 900 °C for 12 h; at the last step, powders again ball milled for 4 h then were pressed as pellets and the pellets heated at 1100 °C for 24 h.

Bruker D8 X-ray diffractometer with  $\text{CuK}\alpha$  source is used to take XRD patterns to analyze the crystalline structure of the samples. Morphology of the samples was examined by SEM using a ZEISS LS 10 model microscope. EIS measurements were taken by Gamry PCI4/750 Potentiostat with an AC signal of 10 mV in the frequency range of  $10^{-1}$ – $10^5$  Hz at room temperature. For this, pellets of the powders with a thickness of 0.9–1 mm and a diameter of 12 mm were pressed by applying a pressure of 43 MPa for 3 minutes, afterwards both sides of pellets were coated with silver and measurements were performed between two stainless steel cylindrical electrodes. X-ray absorption fine structure data were collected at BL8:XAS beamline of the SIAM Photon synchrotron laboratory (SLRI), which is located in Suranaree University, Nakhon Ratschaisima, Thailand [18]. The structure analysis of the solid electrolytes was performed on two parts; XANES (X-ray Absorption Near Edge Spectroscopy) for the electronic properties and EXAFS (Extended-XAFS) for structural characterization by using the software of IFFEFIT package [19].

## 3. Results and discussion

In Figure 2., XRD patterns of  $\text{Li}_{7-3x}(\text{Ga}_{(1-y)}\text{In}_{(y)})_x\text{La}_3\text{Zr}_2\text{O}_{12}$  samples are given comparatively. All patterns show the cubic LLZO crystal XRD peaks except the peak at the angle of 28.8° which is indicated by the colored column.

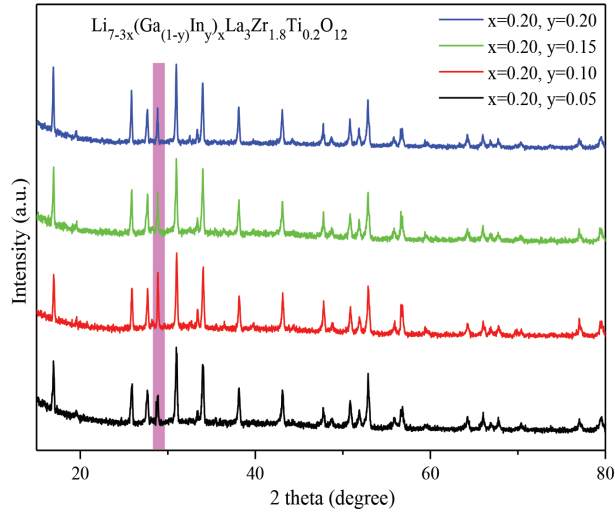


**Figure 2.** XRD patterns of  $\text{Li}_{7-3x}(\text{Ga}_{(1-y)}\text{In}_{(y)})_x\text{La}_3\text{Zr}_{1.8}\text{Ti}_{0.2}\text{O}_{12}$  ( $x=0.20$ ,  $y=0.05, 0.10, 0.15, 0.20$ ) samples comparatively, the peak arising from the second phase is indicated by the colored column.

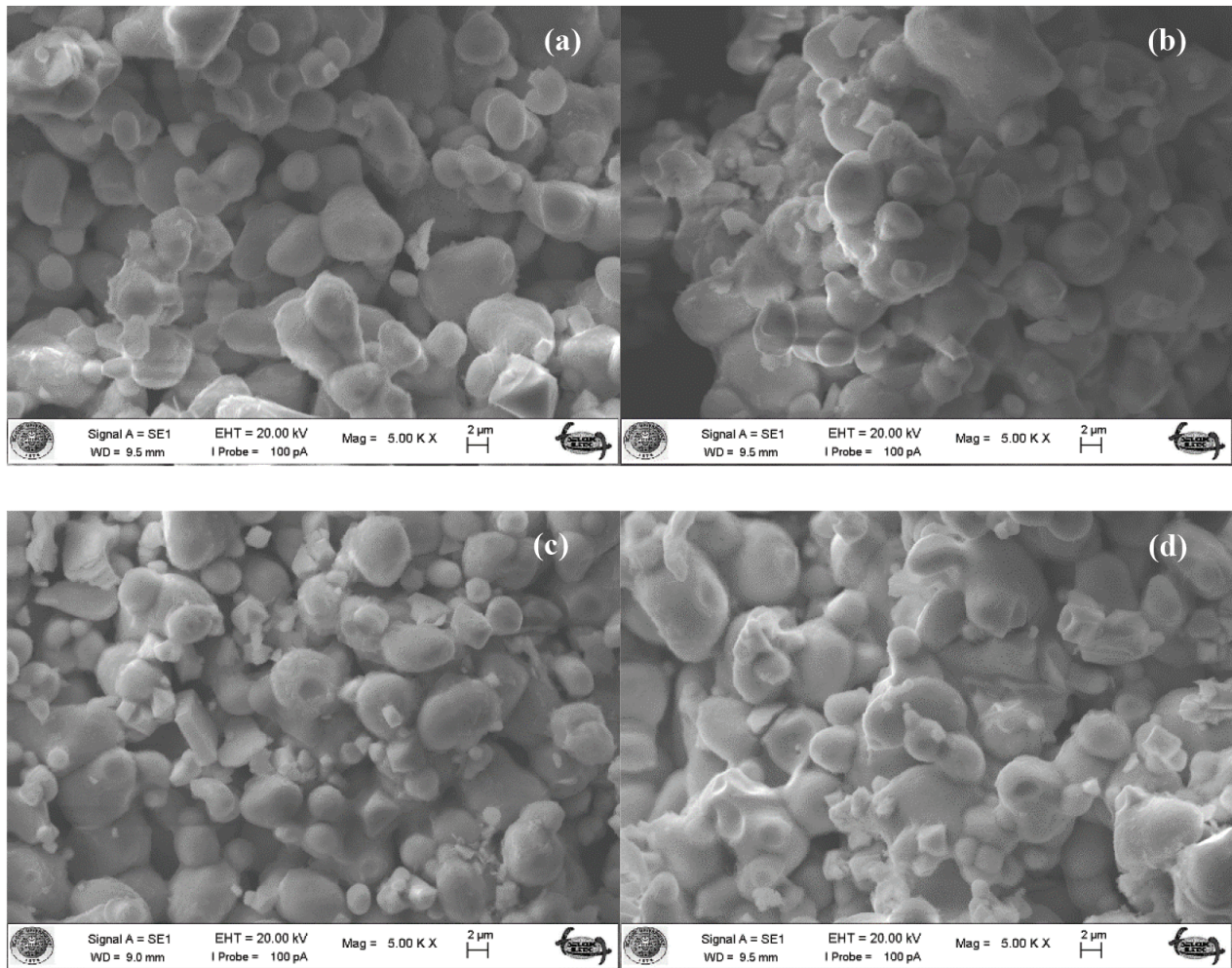
From the comprehensive crystal structure analysis performed with MAUD software (Table 1), it was understood that the peak at  $28.8^\circ$  belonged to the  $\text{La}_2\text{Zr}_2\text{O}_7$  crystal formed as a second phase in the structure [20]. It has been stated in the literature that this second phase is generally due to loss of Li atoms from the structure during sintering [21]. When the normalized XRD patterns are concerned, it is seen that the peak intensity of the second crystal,  $\text{La}_2\text{Zr}_2\text{O}_7$  first increases and then decreases. Since the peak intensity represents the quantity of X-rays reflected from the atoms forms that plane, we can say that the amount of the second crystal formed in the structure with doping first increases and then decreases. The detailed crystal structure analysis confirms the interpretation above by showing that the  $\text{La}_2\text{Zr}_2\text{O}_7$  crystal in the system was formed by 5.04%, 8.02%, 7.07% and 4.55%, as the Ga amount decreased and the In amount increased. Compared to the previous work in which only Ga contribution is made, the presence of In atoms simultaneously with Ga atoms in Li sites created the second unwanted phase although the cubic structure was preserved [22]. The lattice parameter ( $a = 12.90\text{--}12.93 \text{ \AA}$ ) decreases in the presence of In when compared to the lattice parameters ( $a = 12.93\text{--}12.97 \text{ \AA}$ ) of only Ga doped samples. On the other hand, the second phase,  $\text{La}_2\text{Zr}_2\text{O}_7$ , was formed in cubic geometry with a space group of  $\text{Fd-}3\text{m:}1$  and the lattice parameter remained constant independent of the amount of contribution,  $a = 10.79 \text{ \AA}$ .

Micrographs of the  $\text{Li}_{7-3x}(\text{Ga}_{(1-y)}\text{In}_{(y)})_x\text{La}_3\text{Zr}_2\text{O}_{12}$  samples are given in Figure 3. When micrographs are examined, it is like small and sharp-edged particles are sprinkled over the large and smooth ones. These small particles in the system most likely belong to the crystalline structure,  $\text{La}_2\text{Zr}_2\text{O}_7$ , formed as a second phase according to the structure analysis and the large ones belong to the Ga-In doped LLZO. Although there is no distinct change for the shape of LLZO particles with the modification of Ga and In amounts, similar images are observed as in the literature [23-25].

Figure 4. displays the Nyquist representation of electrochemical impedance spectroscopy of  $\text{Li}_{7-3x}(\text{Ga}_{(1-y)}\text{In}_{(y)})_x\text{La}_3\text{Zr}_2\text{O}_{12}$  samples performed in the frequency range of  $10^{-1} \text{ Hz--}100 \text{ kHz}$ . Graphs consist of a single semicircle and a tail extending at low frequency values. Since the point where the semicircle intersects the x-axis gives the real resistance, it is understood that the total ionic resistance in the sample increases with the

**Table 1.** Crystal structure analysis of the  $\text{Li}_{7-3x}(\text{Ga}_{(1-y)}\text{In}_{(y)})_x\text{La}_3\text{Zr}_2\text{O}_{12}$  samples.

| Substitution      | Crystal   | a (Å) | Geometry | Space Group | %(Weight) |
|-------------------|---|-------|----------|-------------|-----------|
| x = 0.2, y = 0.05 | $\text{Li}_{6.64}\text{Ga}_{0.19}\text{In}_{0.01}\text{La}_3\text{Zr}_2\text{O}_{12}$ | 12.92 | Cubic    | I-43d       | 94.96     |
|                   | $\text{La}_2\text{Zr}_2\text{O}_7$  | 10.79 | Cubic    | Fd-3m:1     | 5.04      |
| x = 0.2, y = 0.10 | $\text{Li}_{6.64}\text{Ga}_{0.18}\text{In}_{0.02}\text{La}_3\text{Zr}_2\text{O}_{12}$ | 12.90 | Cubic    | I-43d       | 91.98     |
|                   | $\text{La}_2\text{Zr}_2\text{O}_7$  | 10.79 | Cubic    | Fd-3m:1     | 8.02      |
| x = 0.2, y = 0.15 | $\text{Li}_{6.64}\text{Ga}_{0.17}\text{In}_{0.03}\text{La}_3\text{Zr}_2\text{O}_{12}$ | 12.92 | Cubic    | I-43d       | 92.93     |
|                   | $\text{La}_2\text{Zr}_2\text{O}_7$  | 10.79 | Cubic    | Fd-3m:1     | 7.07      |
| x = 0.2, y = 0.20 | $\text{Li}_{6.64}\text{Ga}_{0.16}\text{In}_{0.04}\text{La}_3\text{Zr}_2\text{O}_{12}$ | 12.93 | Cubic    | I-43d       | 95.45     |
|                   | $\text{La}_2\text{Zr}_2\text{O}_7$  | 10.79 | Cubic    | Fd-3m:1     | 4.55      |

**Figure 3.** Micrographs of the  $\text{Li}_{7-3x}(\text{Ga}_{(1-y)}\text{In}_{(y)})_x\text{La}_3\text{Zr}_2\text{O}_{12}$  samples (a) x = 0.20, y = 0.05, (b) x = 0.20, y = 0.10, (c) x = 0.20, y = 0.15 and (d) x = 0.20, y = 0.20.

increase of In amount. In order to study in detail the grain and grain boundary resistance of the samples, the equivalent circuit in Figure 4 (e) is used to fit the experimental data. The data given with the black line in the graphs belongs to the curve obtained with this equivalent circuit. In Figure 4 (d), the deviation of the data obtained with the fit from the real data may be caused by the silver electrode being prepared for this sample worse than the others or the difficulty to take accurate measurements at very low frequency values. Since the tail at low frequency region is due to the diffusion layer between the pellet (sample) and silver electrode, the deviation does not constitute any problem for the total resistivity of the sample [26].

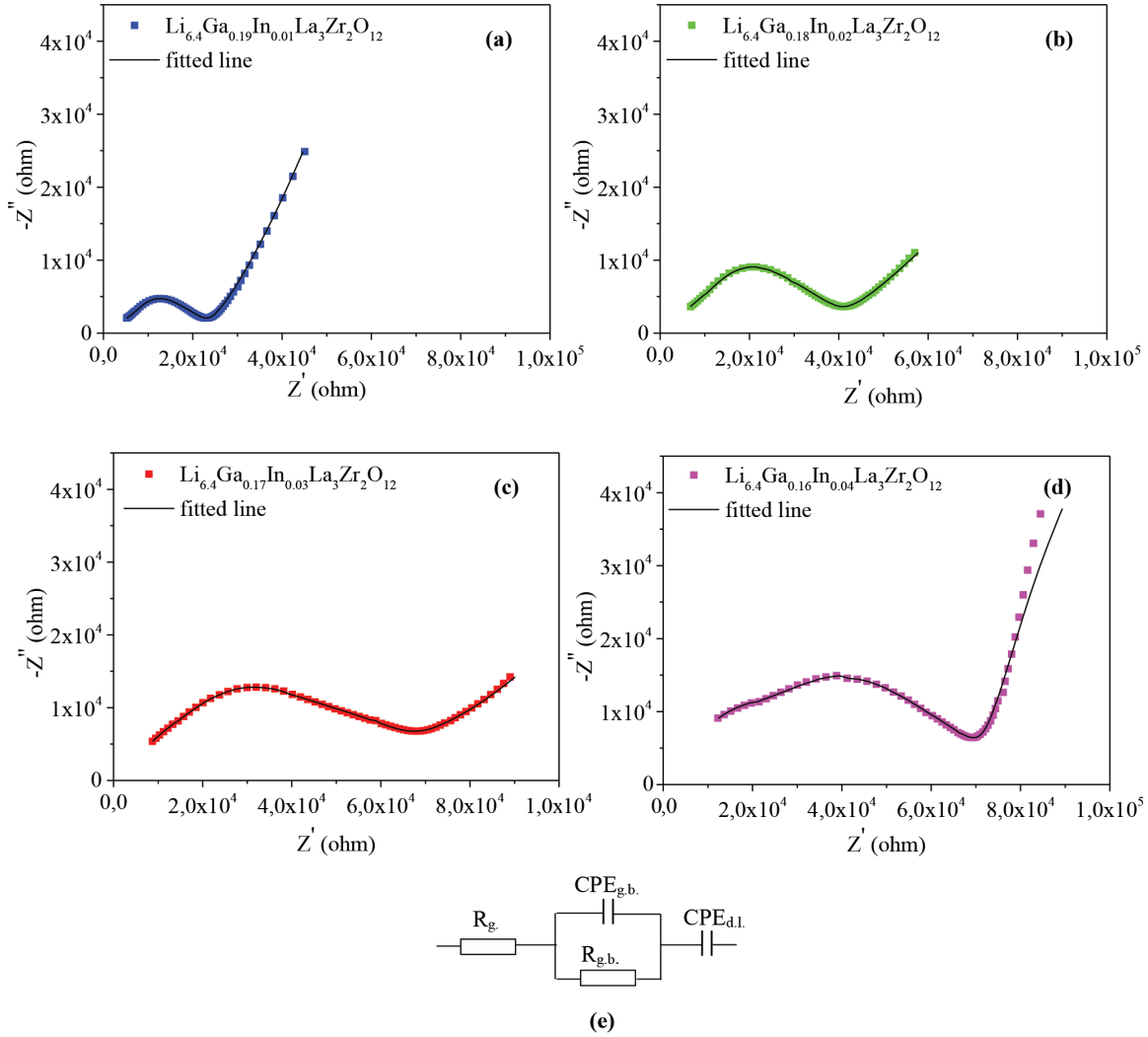


**Figure 4.** Impedance data of the  $\text{Li}_{7-3x}(\text{Ga}_{(1-y)}\text{In}_{(y)})_x\text{La}_3\text{Zr}_2\text{O}_{12}$  samples taken at room temperature and fitted results. (a)  $x = 0.20$ ,  $y = 0.05$ , (b)  $x = 0.20$ ,  $y = 0.10$ , (c)  $x = 0.20$ ,  $y = 0.15$ , (d)  $x = 0.20$ ,  $y = 0.20$ , (e) Schematic representation of the equivalent circuit used to fit experimental data.

The abbreviation of CPE is served as constant phase element whose impedance is given by  $Z_{CPE} = 1/Q(\omega j)^n$ . Here,  $Q$  is a value related to capacitance with the unit  $\text{S.s}^n$ ,  $\omega$  is the frequency,  $n$  is a constant between 0-1 and  $j = \sqrt{-1}$ . Fit results for the values of resistance within grain ( $R_g$ ), resistance between grains ( $R_{g.b.}$ ),  $Q_{g.b.}$ ,  $n_{g.b.}$  and the value of the grain boundary capacitance ( $C_{g.b.}(F)$ ) calculated by the following

equation are summarized in Table 2 [27].

$$C = R^{(1-n)/n} Q^{(1/n)} \quad (3)$$

**Table 2.** Fit results of the impedance data evaluated by using the equivalent circuit given in Figure 4 (e),  $\chi^2$ , square of the standard deviation.

| Sample                                      | $R_g. (\Omega)$       | $R_{g.b.} (\Omega)$ | $Q_{g.b.} (S.s^n)$    | $n_{g.b.}$            | $C_{g.b.} (F)$         | $\chi^2$              |
|---|-----------------------|---------------------|-----------------------|-----------------------|------------------------|-----------------------|
| $Li_{6.64}Ga_{0.19}In_{0.01}La_3Zr_2O_{12}$ | $3.29 \times 10^3$    | $1.98 \times 10^4$  | $1.94 \times 10^{-7}$ | $5.61 \times 10^{-1}$ | $2.82 \times 10^{-9}$  | $3.96 \times 10^{-4}$ |
| $Li_{6.64}Ga_{0.18}In_{0.02}La_3Zr_2O_{12}$ | $3.55 \times 10^3$    | $3.34 \times 10^4$  | $9.15 \times 10^{-8}$ | $5.83 \times 10^{-1}$ | $1.56 \times 10^{-9}$  | $2.27 \times 10^{-4}$ |
| $Li_{6.64}Ga_{0.17}In_{0.03}La_3Zr_2O_{12}$ | $1.67 \times 10^3$    | $5.33 \times 10^4$  | $1.38 \times 10^{-7}$ | $5.11 \times 10^{-1}$ | $1.29 \times 10^{-9}$  | $9.31 \times 10^{-5}$ |
| $Li_{6.64}Ga_{0.16}In_{0.04}La_3Zr_2O_{12}$ | $1.87 \times 10^{-2}$ | $7.32 \times 10^4$  | $1.37 \times 10^{-7}$ | $4.51 \times 10^{-1}$ | $5.05 \times 10^{-10}$ | $1.17 \times 10^{-3}$ |

When we look at the values of  $R_g.$  and  $R_{g.b.}$ , it is seen that the resistance value inside the grain decreases and the resistance value between the grain boundaries increases with the decrease of Ga and the increase of In simultaneously in the sample. For the sample  $Li_{6.64}Ga_{0.16}In_{0.04}La_3Zr_2O_{12}$ , it is understood that the resistance inside the grain goes to zero and the total resistance of the sample is represented by the resistance between the grain boundaries. This actually does not mean that the resistance inside the grain is zero, but that the resistance within the grain and at the grain boundaries cannot be distinguished from each other and the resistance of the sample is actually expressed with a single value. The increase in the resistance between the grain boundaries with the increase of In may be a consequence of the decrease in the density of the sample due to different additive amounts [2]. Typical grain boundary capacitance values in the literature are given in the  $10^{-11}$ - $10^{-8}$  F range [28]. The compatibility of the grain boundary capacitance values obtained in this study with the literature indicates that the microstructure is also homogeneously distributed. In previous studies, it is stated that higher capacitance values were encountered in well-sintered samples, while lower capacitance values were encountered in poorly-sintered samples [28,29]. When we look at the grain boundary capacitance values of the samples in this study, the capacitance values decrease with the increase of In amount. As stated above, the reason for this decrease is possibly that the increase in In amount affected the sintering quality adversely and consequently the densities.

Total ionic conductivity of the  $Li_{6.64}Ga_{0.19}In_{0.01}La_3Zr_2O_{12}$ ,  $Li_{6.64}Ga_{0.18}In_{0.02}La_3Zr_2O_{12}$ ,  $Li_{6.64}Ga_{0.17}In_{0.03}La_3Zr_2O_{12}$  and  $Li_{6.64}Ga_{0.16}In_{0.04}La_3Zr_2O_{12}$  samples are calculated by the following equation.

$$\sigma = (1/R)(l/a) \quad (4)$$

as  $4.39 \times 10^{-6}$  S.cm<sup>-1</sup>,  $2.74 \times 10^{-6}$  S.cm<sup>-1</sup>,  $1.93 \times 10^{-6}$  S.cm<sup>-1</sup> and  $1.37 \times 10^{-6}$  S.cm<sup>-1</sup>, respectively. Here,  $R$  is the total resistance,  $l$  is the thickness, and  $a$  is the area of the pellet.

As In dopant may have an effect on the decrease of density, it may also have blocked the ion pathways by affecting the Li ion space distribution pattern. However, in this study, since the In atoms which are partially replaced by Ga atoms affected the grain boundary resistance as it can be understood from the capacitance values too, In atoms more likely to have an influence on the density of the samples. The entity of In in the

structure leads LLZO material to form in a less dense with a cubic structure and a low total ionic conductivity at room temperature as compared to the Ga substituted LLZO material.

In Figure 5, normalized In  $L_3$ -edge XANES spectra are given comparatively.  $L_3$ -edge absorption spectra are the transition mechanism of the excited  $2p_{3/2}$  electrons to the empty  $5s$  levels. In the Figure, the thin In metal layer is used as the reference material to make it easy to observe the electronic response of indium atoms substituted in gallium positions. The band energy level formed by the valence electrons of two different atoms in the molecule can split into low energy ( $t_{2g}$ ) level and high energy ( $e_g$ ) level. Considering this situation, the absorption spectrum of indium foil which has a smooth edge feature, starts to increase at 3727 eV and switch to the low energy level ( $t_{2g}$ ) of s levels at 3733 eV. However, In substituted LLZO materials have multiple peak properties when compared to metallic indium. This is the result of hybridization of the s-levels of the source atom with the valence orbitals of neighboring atoms. This multiple peak location at the absorption edge is related to the oxidation states of indium in its environment. The multiple peak at 3732 eV confirms the presence of low energy molecular levels of 5s levels, while the peak around 3734.3 eV reveals the presence of high energy molecular levels.

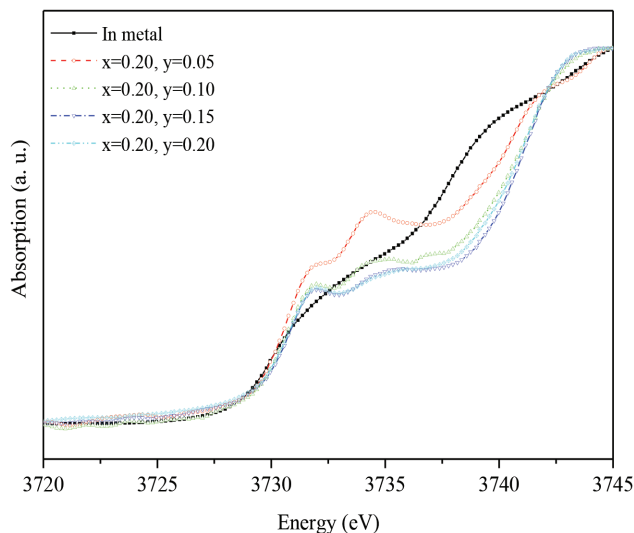


**Figure 5.** In  $L_3$ -edge XANES spectra of the  $\text{Li}_{7-3x}(\text{Ga}_{(1-y)}\text{In}_{(y)})_x\text{La}_3\text{Zr}_2\text{O}_{12}$  samples.

Comparison of the scattering intensities obtained from the EXAFS spectra of the LLZO materials with 10% and 20% indium substituted to gallium coordination is given in Figure 6. The harmony between the data of 10% and 20% In substituted LLZO material is remarkable. The fact that the increase of indium amount within the structure does not cause a shift in the scattering data graph can be explained by the small amount of indium atoms added and not having the power to have a structural effect (for the  $x = 0.20$ ,  $y = 0.10$  values, the molar ratio of Ga and In atoms,  $\text{Ga}/\text{In} = 9$ , and for the  $x = 0.20$ ,  $y = 0.20$  values, the molar ratio of Ga and In atoms,  $\text{Ga}/\text{In} = 4$ ). The parallel coherence of the data in the Figure indicates structural similarities. Also, the distortion at high  $k$  values highlights the strong inter-atomic potential that causes a high drop in the kinetic energy of photo electrons traveling between neighboring atoms. It is clear that the heavy indium atoms will have a high contribution to the potential of the medium. From this point, the scattering of the photo electrons emitted by indium atoms from the heavy atoms surrounding them and moving in the high potential environment is the reason for the damping in their energy.



The reflection of the scattering intensities of the radial distribution of the atoms on a one-dimensional axis of the samples is given in Figure 7. In the graph, the high agreement of the radial distribution spectra obtained from the LLZO materials with 10% and 20% indium substituted to the gallium coordinations shows that there is almost no change in the crystal structure and in the atomic positions of both materials. Despite the high variability in the electronic structure, this situation does not cause a structural deterioration due to the weak effects in the new settlements of indium atoms and reveals their harmony.

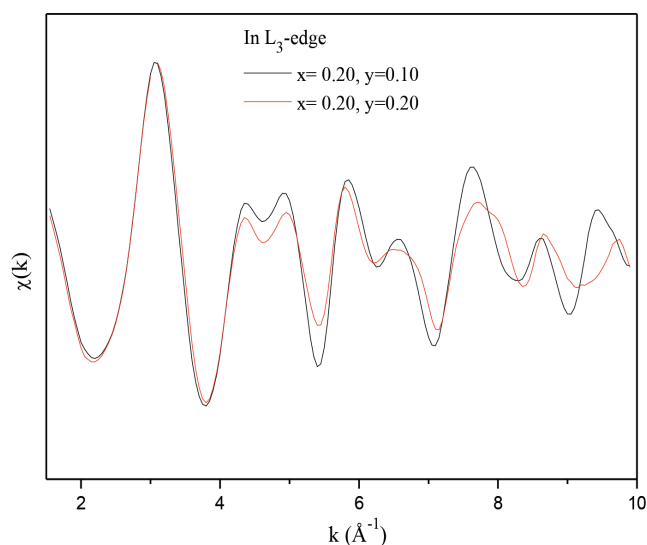


**Figure 6.** The In  $L_3$ -edge EXAFS scattering intensity of the  $\text{Li}_{7-3x}(\text{Ga}_{(1-y)}\text{In}_{(y)})_x\text{La}_3\text{Zr}_2\text{O}_{12}$  samples.

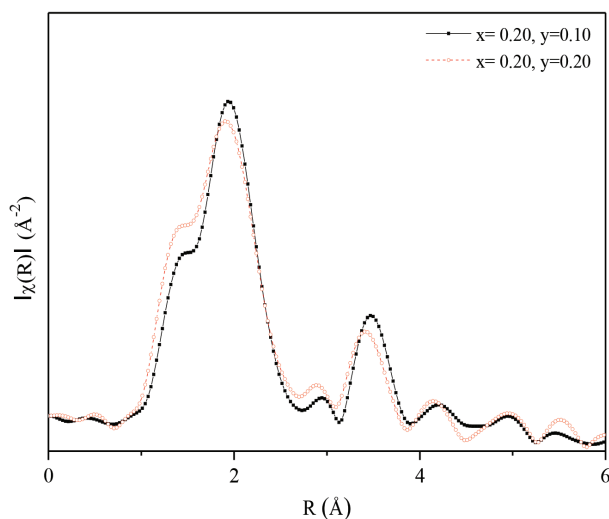


**Figure 7.** The radial distribution function of the In  $L_3$ -edge scattering intensities of the  $\text{Li}_{7-3x}(\text{Ga}_{(1-y)}\text{In}_{(y)})_x\text{La}_3\text{Zr}_2\text{O}_{12}$  samples.

#### 4. Conclusion

In this study, LLZO solid electrolytes in which two different atoms are located in Li sites are discussed. As understood from the crystal structure analysis, although the samples reached a cubic structure, a tiny amount

of a different crystal structure,  $\text{La}_2\text{Zr}_2\text{O}_7$ , is also formed in the system. The total ionic conductivity of the samples decreased with the increase of In amount at the same  $\text{Li}^+$  ion concentration, indicating that the entity of In atoms within the structure reduce the mobility of the  $\text{Li}^+$  ions. Analysis of impedance data showed that increasing the amount of In might have reduced the density of the samples which effects the mobility of  $\text{Li}^+$  ions at the grain boundaries, showing that the highest conductivity was obtained in the sample with the least amount of In. Since the amount of In atoms compared to Ga atoms are very less in the structure, they did not have a structural effect, and, therefore, no strong change in the scattering graphs was observed. On the other hand, the fact that the RDF graphs are also symmetrical, it is understood that the samples are formed in the same crystal structure independent of the In amount.

### Acknowledgment

The authors gratefully acknowledge the financial support of “17101004” project of Selçuk University Scientific Research Projects (BAP) Coordinating Office (Konya, Turkey).

### References

- [1] Wu JF, Chen EY, Yu Y, Liu L, Wu Y et al. Gallium-Doped  $\text{Li}_7\text{La}_3\text{Zr}_2\text{O}_{12}$  garnet-type electrolytes with high lithium-ion conductivity. *Acs Applied Materials & Interfaces* 2017; 9 (2): 1542-1552. doi: 10.1021/acsami.6b13902
- [2] Posch P, Lunghammer S, Berendts S, Ganschow S, Redhammer GJ et al. Ion dynamics in Al-Stabilized  $\text{Li}_7\text{La}_3\text{Zr}_2\text{O}_{12}$  single crystals - Macroscopic transport and the elementary steps of ion hopping. *Energy Storage Materials* 2020; 24: 220-228. doi: 10.1016/j.ensm.2019.08.017
- [3] Rettenwander D, Langer J, Schmidt W, Arrer C, Harris KJ et al. Site occupation of Ga and Al in Stabilized Cubic  $\text{Li}_{7-3(x+y)}\text{Ga}_x\text{Al}_y\text{La}_3\text{Zr}_2\text{O}_{12}$  garnets as deduced from  $(27) \text{Al}$  and  $\text{Ga}$ -71 MAS NMR at ultrahigh magnetic fields. *Chemistry of Materials* 2015; 27 (8):3135-3142. doi: 10.1021/acs.chemmater.5b00684
- [4] Jalem R, Rushton MJD, Manalastas W, Nakayama M, Kasuga T et al. Effects of Gallium doping in garnet-type  $\text{Li}_7\text{La}_3\text{Zr}_2\text{O}_{12}$  solid electrolytes. *Chemistry of Materials* 2015; 27 (8): 2821-2831. doi: 10.1021/cm5045122
- [5] Xiang X, Liu Y, Chen F, Yang WY, Yang JB et al. Crystal structure and lithium ionic transport behavior of Li site doped  $\text{Li}_7\text{La}_3\text{Zr}_2\text{O}_{12}$ . *Journal of the European Ceramic Society* 2020; 40 (8):3065-3071. doi: 10.1016/j.jeurceramsoc.2020.02.054
- [6] Wagner R, Redhammer GJ, Rettenwander D, Senyshyn A, Schmidt W et al. Crystal structure of garnet-related Li-Ion Conductor  $\text{Li}_{7-3x}\text{Ga}_x\text{La}_3\text{Zr}_2\text{O}_{12}$ : fast li-ion conduction caused by a different cubic modification?. *Chemistry of Materials* 2016; 28 (6):1861-1871. doi: 10.1021/acs.chemmater.6b00038
- [7] Rettenwander D, Blaha P, Laskowski R, Schwarz K, Bottke P et al. DFT Study of the Role of  $\text{Al}^{3+}$  in the Fast Ion-Conductor  $\text{Li}_{7-3x}\text{Al}_x\text{La}_3\text{Zr}_2\text{O}_{12}$  Garnet. *Chemistry of Materials* 2014; 26 (8): 2617-2623. doi: 10.1021/cm5000999
- [8] Rettenwander D, Geiger CA, Tribus M, Tropper P, Amthauer G. A Synthesis and crystal chemical study of the fast ion conductor  $\text{Li}_{7-3x}\text{Ga}_x\text{La}_3\text{Zr}_2\text{O}_{12}$  with  $x=0.08$  to  $0.84$ . *Inorganic Chemistry* 2014; 53 (12): 6264-6269. doi: 10.1021/ic500803h
- [9] Xiang X, Chen F, Shen Q, Zhang LM, Chen CL. Effect of the lithium ion concentration on the lithium ion conductivity of Ga-doped LLZO. *Materials Research Express* 2019; 6 (8). doi: 10.1088/2053-1591/ab2799
- [10] Wolfenstine J, Ratchford J, Rangasamy E, Sakamoto J, Allen JL. Synthesis and high Li-ion conductivity of Ga-stabilized cubic  $\text{Li}_7\text{La}_3\text{Zr}_2\text{O}_{12}$ . *Materials Chemistry and Physics* 2012; 134 (2-3): 571-575. doi: 10.1016/j.matchemphys.2012.03.054
- [11] Shin DO, Oh K, Kim KM, Park KY, Lee B et al. Synergistic multi-doping effects on the  $\text{Li}_7\text{La}_3\text{Zr}_2\text{O}_{12}$  solid electrolyte for fast lithium ion conduction. *Scientific Reports* 2015; 5. doi: 10.1038/srep18053

- [12] Wang C, Lin PP, Gong Y, Liu ZG, Lin TS et al. Co-doping effects of Ba<sup>2+</sup> and Ta<sup>5+</sup> on the microstructure and ionic conductivity of garnet-type solid state electrolytes. *Journal of Alloys and Compounds* 2021; 854. doi: 10.1016/j.jallcom.2020.157143
- [13] Cao Z, Li Y, Su J, Zhao J, Li Y et al. Y and Sb co-doped Li<sub>7</sub>La<sub>3</sub>Zr<sub>2</sub>O<sub>12</sub> electrolyte for all solid-state lithium batteries. *Ionics* 2021. doi: 10.1007/s11581-021-03919-z
- [14] Dubey BP, Sahoo A, Thangadurai V, Sharma Y. Morphological, dielectric and transport properties of garnet-type Li<sub>6.25+y</sub>Al<sub>0.25</sub>La<sub>3</sub>Zr<sub>2-y</sub>MnyO<sub>12</sub> (y=0, 0.05, 0.1, and 0.2). *Solid State Ionics* 2010; 351. doi: 10.1016/j.ssi.2020.115339
- [15] Abrha LH, Hagos TT, Nikodimos Y, Bezabh HK, Berhe GB et al. Dual-doped cubic garnet solid electrolytes with superior air stability. *ACS Applied Materials & Interfaces* 2020; 12 (23): 25709-25717. doi: 10.1021/acsami.0c01289
- [16] Karasulu B, Emge SP, Groh MF, Grey CP, Morris AJ. Al/Ga-Doped Li<sub>7</sub>La<sub>3</sub>Zr<sub>2</sub>O<sub>12</sub> garnets as Li-ion solid-state battery electrolytes: atomistic insights into local coordination environments and their influence on O-17, Al-27, and Ga-71 NMR Spectra. *Journal of the American Chemical Society* 2020; 142 (6): 3132-3148. doi: 10.1021/jacs.9b12685
- [17] Zhang YH, Chen F, Tu R, Shen Q, Zhang XL et al. Effect of lithium ion concentration on the microstructure evolution and its association with the ionic conductivity of cubic garnet-type nominal Li<sub>7</sub>Al<sub>0.25</sub>La<sub>3</sub>Zr<sub>2</sub>O<sub>12</sub> solid electrolytes. *Solid State Ionics* 2016; 284: 53-60. doi: 10.1016/j.ssi.2015.11.014
- [18] Klysubun W, Tarawarakam P, Sombunchoo P, Klinkhieo S, Chaiprapa J et al. X-ray absorption spectroscopy beamline at the Siam Photon Laboratory. *Synchrotron Radiation Instrumentation, Pts 1 and 2* 2017; 879:860.
- [19] Newville M. IFEFFIT: interactive XAFS analysis and FEFF fitting. *Journal of Synchrotron Radiation* 2001; 8: 322-324. doi: 10.1107/S0909049500016964
- [20] Lutterotti L. Maud: a Rietveld analysis program designed for the internet and experiment integration. *Acta Crystallographica a-Foundation and Advances* 2000; 56: S54-S54. doi: 10.1107/S0108767300021954
- [21] Paoletta A, Zhu W, Bertoni G, Savoie S, Feng ZM et al. Discovering the Influence of Lithium Loss on Garnet Li<sub>7</sub>La<sub>3</sub>Zr<sub>2</sub>O<sub>12</sub> Electrolyte Phase Stability. *ACS Applied Energy Materials* 2020; 3 (4): 3415-3424. doi: 10.1021/acsaem.9b02401
- [22] Aktas S, Ozkendir OM, Eker YR, Ates S, Atav U et al. Study of the local structure and electrical properties of gallium substituted LLZO electrolyte materials. *Journal of Alloys and Compounds* 2019; 792:279-285. doi: 10.1016/j.jallcom.2019.04.049
- [23] Cao ZZ, Wu WW, Li Y, Zhao JJ, He WY et al. Lithium ionic conductivity of Li<sub>7-3x</sub>FexLa<sub>3</sub>Zr<sub>2</sub>O<sub>12</sub> ceramics by the Pechini method. *Ionics* 2020; 26 (9): 4247-4256. doi: 10.1007/s11581-020-03580-y
- [24] Li CL, Liu YF, He J, Brinkman KS. Ga-substituted Li<sub>7</sub>La<sub>3</sub>Zr<sub>2</sub>O<sub>12</sub>: An investigation based on grain coarsening in garnet-type lithium ion conductors. *Journal of Alloys and Compounds* 2017; 695: 3744-3752. doi: 10.1016/j.jallcom.2016.11.277
- [25] Afyon S, Krumeich F, Rupp JLM. A shortcut to garnet-type fast Li-ion conductors for all-solid state batteries. *Journal of Materials Chemistry A* 2015; 3 (36): 18636-18648. doi: 10.1039/c5ta03239c
- [26] Walter GW. A Review of impedance plot methods used for corrosion performance analysis of painted metals. *Corrosion Science* 1986; 26 (9): 681-703. doi: 10.1016/0010-938x(86)90033-8
- [27] Haile SM, West DL, Campbell J. The role of microstructure and processing on the proton conducting properties of gadolinium-doped barium cerate. *Journal of Materials Research* 1998; 13 (6): 1576-1595. doi: 10.1557/Jmr.1998.0219
- [28] Irvine JTS, Sinclair DC, West AR. Electroceramics: characterization by impedance spectroscopy. *Advanced Materials* 1990.
- [29] Bruce PG, West AR. The AC conductivity of polycrystalline lithium, Li<sub>2+2xzn1-X</sub>geo<sub>4</sub>, and a model for intergranular constriction resistances. *Journal of the Electrochemical Society* 1983; 130 (3): 662-669. doi: 10.1149/1.2119778